2021 IEEE International Conference on Robotics and Automation (ICRA 2021)
May 31 - June 4, 2021, Xi'an, China

A Flexible Magnetic Field Mapping Model For Calibration of Magnetic Manipulation System

Yi Xing, Yanchao Jia, Zhen Zhan, Jianjie Li and Chengzhi Hu*, *Member, IEEE*

***Abstract*— Magnetic manipulation provides a versatile, remote, noninvasive, and cost-effective strategy in a variety of applications. Till now, many different configurations of magnetic manipulation systems have been developed to address different needs on force, torque, accuracy, and accessibilities. Magnetic field mapping can help to explore the exact map of the magnetic field in the working space and guarantee the homogeneity of the magnetic field. In this paper, a flexible mapping method is employed to solve the scalar potential of the magnetic source by using the separation of variables in Cartesian coordinates. Levenberg-Marquardt Algorithm (LMA) and Whale Optimization Algorithm (WOA) are set to the solver of the model. The work is evaluated in the mapping of an eight-pole magnetic manipulation system. The result of numerical simulation shows that the coefficient of determination R^2 of the model reaches 99.81%, and the actual system mapping obtains R^2 value of 99.57%. This technique can directly be used to calculate the magnetic flux density and gradient field in a short period (≈1ms). Finally, the manipulation of a permanent magnet under the control magnetic field mapping and PID controller demonstrates the effectiveness of the proposed method.**

I. Introduction

Magnetic manipulation of micro- and nanoscale objects has gained great attention for the delicate operations in the field of targeted drug delivery [1], [2] and minimally invasive surgeries [3], [4]. Magnetic manipulation can achieve wireless, non-invasive and precise actuation at small scale, and it is insensitive to biological substances, enabling the *ex vivo* actuation for *in vivo* applications. Magnetic manipulation can be easily conducted by permanent magnets [5], Helmholtz coils [6], [7], Maxwell coils [8], magnetic resonance imaging (MRI) systems [9], and other customized electromagnetic coils [10], [11]. By mounting permanent magnets on robotic arms, magnetic manipulators by single rotating-permanent-magnet or multiple permanent magnets have proved viable options for wireless actuation. Multiple magnets are introduced to produce magnetic fields with high uniformity for torque actuations. Commercial magnetic manipulation, such as Niobe by Stereotaxis [12], has achieved precise orientation control for guiding magnetic catheters. Compared with the permanent magnets, electromagnetic actuation provides high flexibility to control the strength and direction of the magnetic fields, thus, different magnetic forces or magnetic torques can be applied by regulating the current in the coils [6]. Electromagnetic systems, such as MRI and customized magnetic manipulation systems consisting of several electromagnetic coils in optimized configurations, employ the superimposition of different magnetic fields. With the development of superconducting technology, superconducting electromagnets have been developed for strong and homogeneous magnetic fields.

Magnetic field mapping is to obtain the exact map of magnetic field to control the spatial and temporal distribution of magnetic fields in the working space [13]. Magnetic field mapping can guarantee the homogeneity of the magnetic field, which is crucial for the analysis, design, and applications of different magnetic manipulation systems. For the case of MRI, a field inhomogeneity of even 3.35 ppm can cause sever geometric and intensity distortion in the reconstructed images. Similarly, the magnetic field distribution of magnetic manipulation systems will affect the dexterity, maneuverability and precision. Correction of magnetic field via different calibration platforms are possible but require knowledge of the magnitude and spatial extent of the magnetic field perturbation.

Magnetic field mapping can be obtained either experimentally or theoretically. However, it is hard to find analytic equations to describe the induced magnetic field for electromagnetic systems that have arbitrary geometries. Interpolation and mathematic fitting have been two widely used methods for magnetic field mapping [14]. In the interpolation, magnetic fields at the different points in space are measured. Since the magnetic field is continuous, the magnetic fields of arbitrary points can be estimated by the interpolation of the known values from the measured points [15]. As a powerful tool in statistics, many interpolation methods can be used, such as linear interpolation, nearest neighbour interpolation, cubic spline interpolation, thin-plate spline interpolation, etc. However, a sufficiently large numbers of measurement points are needed to ensure the accuracy of magnetic mapping. The interpolation method is not effective for dealing with gradient error or the overall continuity of the magnetic fields [16]. Apart from these, different types of interpolation methods also provide different effectiveness and accuracy during the implementation [17]. In the mathematical fitting, measurement data are used to fit the mathematic functions. A major problem in using mathematical fitting is the selection of an appropriate type of function that best fits the measurement data. Mathematical fitting of electromagnetic systems is generally based on the

The financial support from the National Natural Science Foundation of China (61903177) and the Shenzhen Science and Technology Program (Grant No. JCYJ20190809144013494) are gratefully acknowledged.

Y. Xing, Y. Jia, Z. Zhan, J. Li and C. Hu are with the Department of Mechanical Engineering and Energy, Southern University of Science and Technology, 518055, China.

C. Hu is with the Guangdong Provincial Key Laboratory of Human-Augmentation and Rehabilitation Robotics in Universities, Southern University of Science and Technology, 518055, China.(Corresponding to: *hucz@sustech.edu.cn*)

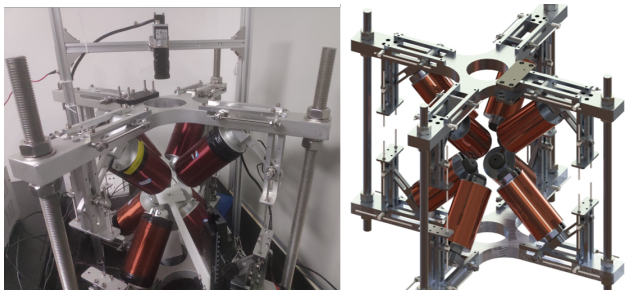

Fig. 1. *Left:* Eight-pole electromagnetic manipulation system. The upper four coils and the lower coil are symmetrical about the horizontal plane, and the angle between the common axis of coil and the horizontal plane is 45°. The system has a total of $(20 \times 20 \times 20\,\mathrm{mm}^3)$ working space and about $(100 \times 100 \times 100\,\mathrm{mm}^3)$ physical space (The maximum size of the object that the system can place). The coil is designed with 1500 turns of 1.5mm copper wire, and the core material is DT4E. *Right:* A rendering of the magnetic manipulation system.

Biot-Savart Law [18]. Previously, Kummer [4] has used the first-order dipole approximation that is based on the magnetic dipole model and fitted the magnetic field data obtained from a finite element method model of the magnetic manipulation system. Such implementation is easy and fast, and needs less measurement points compared to the interpolation method. With the developed mathematical model, it is convenient to predict the magnetic field in the space. However, the accuracy can be greatly affected by the choose of different fitting models as well as the strategy for choosing the measurement points for fitting.

This paper introduces a flexible magnetic field mapping model based on a general solution to the Laplace equation. The model has smooth property and satisfies the curl and divergence of the magnetic field. A magnetic manipulation system with eight electromagnets is shown in Fig. 1. The simulation data by FEA and actual measurement data of the magnetic field from the developed magnetic manipulation system are used to verify the effectiveness of the mapping model. Using this method, it is able to obtain magnetic field information of the magnetic manipulation system with respect to coordinates and current in a very short period of time (≈1ms), and achieve precise manipulation of magnetic objects.

II. Magnetic Field Mapping Model of Magnetic Manipulation System In Situ

When there is no magnetic source in the working space of the magnetic manipulation system, Maxwells equation can be written as follows [16]

$$\nabla \cdot \mathbf{B} = 0 \tag{1}$$

$$\nabla \times \mathbf{H} = 0 \tag{2}$$

where $\mathbf{B}(x, y, z) \in \mathbb{R}^3$ is the magnetic flux density and $\mathbf{H}(x, y, z) \in \mathbb{R}^3$ is the magnetic field strength. In order to solve the constraints in equation (1)-(2), magnetic charge model is used to analyse the distribution of the magnetic field in the free space, thus the magnetic field strength and magnetic flux density can be expressed by the first order spatial derivative of a scalar potential

$$\mathbf{B} = \mu_0 \mathbf{H} = -\mu_0 \nabla \Phi \tag{3}$$

where $\mu_0 = 4\pi \times 10^{-7}\,\mathrm{T \cdot m/A}$ is the permeability of free space. From (1)-(3) the magnetic scalar potential can be described as

$$\nabla^2 \Phi = 0 \tag{4}$$

(4) is the Laplace equation, and thus the magnetic field developed by the magnetic scalar potential satisfies the constrain equation in the Maxwell equations. For a magnetic manipulation system in Cartesian coordinates, as shown in Fig. 1. The commonly used method is polynomial regression, but the higher-order terms of the solution do not satisfy the Laplace equation. To deal with this issue, the solution uses only the lower-order terms as

$$\varphi_{pr}(x, y, z) = tr(\mathbb{A}\Upsilon) + a_{111}xyz + a_0 \tag{5}$$

and

$$\mathbb{A} = \begin{bmatrix} a_{100} & a_{010} & a_{001} \\ a_{110} & a_{101} & a_{011} \\ a_{200} & a_{020} & a_{002} \end{bmatrix}$$

$$\Upsilon = \begin{bmatrix} x & xy & x^2 \\ y & xz & y^2 \\ x & yz & z^2 \end{bmatrix}$$

where $\varphi_{pr}(x, y, z)$ is the polynomial solution to Laplace equation at point (x, y, z) in Cartesian coordinates, tr represents the trace of the matrix, $\mathbb{A}$ is the coefficient matrix and the subscript numbers in $\mathbb{A}$ represent the power of each term. The product of three single variables satisfies the Laplace equation. a_0 is the constant term in polynomial that has no practical meaning. It should be noticed that the combination of the quadratic terms which contains only single variables does not satisfy the Laplace equation. But when the addition of coefficients equals to zero, the constructed solution still satisfies the basic solution to the Laplace equation. That is

$$a_{200} + a_{020} + a_{002} = 0 \tag{6}$$

In a multi-pole magnetic manipulation system, the mutual influence between magnetic sources is not neglectable, making it impossible for the magnetic field developed by single electromagnet to be uniform or homogeneous (Data not shown). Low-order polynomial regression cannot accurately describe the complex magnetic field distribution. Due to the linearity of the Laplace equation, a more general solution to the Laplace equation is proposed as [19]

$$\begin{aligned} \Phi(x, y, z) &= \sum_{p=1}^{K} c_p \varphi_p(x, y, z) + \varphi_{pr} \\ &= \sum_{p=1}^{K} c_p L_p(x) M_p(y) N_p(z) + \varphi_{pr} \end{aligned} \tag{7}$$

$$L_p(x) = (l_{1p}\sinh(k_{1p}x) + l_{2p}\cosh(-k_{1p}x))$$
$$M_p(y) = (m_{1p}\sin(k_{2p}y) + m_{2p}\cos(-k_{2p}y))$$
$$N_p(z) = (n_{1p}\sin(k_{3p}z) + n_{2p}\cos(-k_{3p}z))$$

and

$$k_{1p}{}^2 + k_{2p}{}^2 + k_{3p}{}^2 = 0, p = 1, 2, ..., K \tag{8}$$

The constants k_{1p}, k_{2p}, k_{3p} are the eigenvalues and $L_p(x)$, $M_p(x)$, $N_p(x)$ are the eigenfunctions, respectively. l_{1p}, l_{2p}, m_{1p}, m_{2p}, n_{1p}, n_{2p} is the constant of the solution, K is the total number of combination solution, which will be discussed in the next section. Obviously, the scalar potential of the mapping region is not a symmetrical situation with respect to x, y, and z, so there are both sin terms and cos terms in the model. The choice of eigenfunction is based on the structural symmetry of the actual system. The number of eigenfunctions and eigenvalues is $6K$ and $3K$, respectively. Substitute (7) into (3), thus the magnetic mapping functions

$$B_x = -\mu_0\frac{\partial\Phi}{\partial x} = (-\mu_0)\sum_{p=1}^{K} c_p M_p(y)N_p(z)\frac{\partial L_p(x)}{\partial x} + \frac{\partial\varphi_{pr}}{\partial x} \tag{9}$$

$$B_y = -\mu_0\frac{\partial\Phi}{\partial y} = (-\mu_0)\sum_{p=1}^{K} c_p L_p(x)N_p(z)\frac{\partial M_p(y)}{\partial y} + \frac{\partial\varphi_{pr}}{\partial y} \tag{10}$$

$$B_z = -\mu_0\frac{\partial\Phi}{\partial z} = (-\mu_0)\sum_{p=1}^{K} c_p L_p(x)N_p(z)\frac{\partial N_p(z)}{\partial z} + \frac{\partial\varphi_{pr}}{\partial z} \tag{11}$$

The mapping function is continuous, so that the gradient matrix can be derived by calculating the partial derivative.

III. Optimal Model of Magnetic Manipulation System Mapping

When the eight-pole magnetic manipulation system is working, the magnetic field distribution can be expressed as a linear superposition of the contribution from each electromagnet. In addition, each electromagnet in Fig.1 is identical in design. The outer diameter is 80 mm, the inner diameter is 40 mm, the length is 125 mm, and the length of the iron core is 150 mm. Therefore, the mathematical model of the entire system's magnetic field is expressed as following

$$\begin{aligned}\mathbf{B}(\mathbf{P}, I) &= \sum_{i=1}^{n}\mathbf{B}^i(\mathbf{P}) + \mathbf{B}_d(P) + \delta_{\mathbf{B}(\mathbf{P})} \\ &= \sum_{i=1}^{n}\mathbf{b}^i(\mathbf{P})I_i + \mathbf{B}_d(P) + \delta_{\mathbf{B}(\mathbf{P})}\end{aligned} \tag{12}$$

where n is the number of electromagnet (with ferromagnetic iron core, in this case $n = 8$), and $\mathbf{B}^i(\mathbf{P})$ is the magnetic field distribution of the ith electromagnet with applied current I_i at point $\mathbf{P}$, and $b^i(\mathbf{P}) \in \mathbb{R}^3$ is the vector magnetic field generated by unit current, $\mathbf{B}_d(P)$ is the external interference to mapping field, its amplitude is relatively small and can be neglected. $\delta_{\mathbf{B}(\mathbf{P})}$ is the vector DC offset.

The magnetic mapping function by solving the Laplace equation has been constructed (9)-(11). As long as the constants in the equation are obtained and the total number of the combination solution K is determined, thus, the magnetic field strength and field gradient at any point in the mapping region can be obtained. While solving the system of nonlinear multi-variable equations, the general approach is to transform it into a fitting model or an optimization model. The actual or simulated magnetic field strength value of the data point in the working space can be obtained through measurement or FEA simulation. In order to avoid the situation that the residual error is small but the relative error is large, the optimization objective is the relative error

$$\begin{aligned}\min_{P_s}\quad & \sum_{M}\sum_{N}\left[\frac{\widehat{B}_{mn}(\mathbf{P}, I) - B_{mn}(\mathbf{P}, I)}{B_{mn}(\mathbf{P}, I)}\right]^2, N = x, y, z \\ \text{s.t.}\quad & lb \le P_s \le ub \\ & a_{200} + a_{020} + a_{002} = 0 \\ & k_{1p}{}^2 + k_{2p}{}^2 + k_{3p}{}^2 = 0,\ p = 1, 2, ..., K\end{aligned}$$

M is the sum of the sampling points, $\widehat{B}_{mn}(\mathbf{P}, I)$ is the output of the magnetic mapping function at point $\mathbf{P}$ with N representing x, y or z component. $B_{mn}(\mathbf{P}, I)$ is the fitting data in x- y- or z- component of the magnetic field which is measured or obtained by the FEA, P_S is the vector stack of the parameters within the lower boundary (*lb*) and upper boundary (*ub*).

1)Levenberg-Marquardt Algorithm (LMA) and Whale Optimization Algorithm (WOA)

For the above high-dimensional nonlinear optimization problem, a combination of LMA and Meta-heuristic optimization algorithm (WOA) [20] is chosen as the mathematical solver, and the constraints are directly modified into the mapping function. In the process of LMA, a global convergence algorithm based on the trust region technique is employed to update the damping coefficient in each iteration [21]–[23]

$$\lambda_k = \alpha_k(\theta\,\|F_k\| + (1-\theta)\,\|J_k{}^T F_k\|) \tag{13}$$

where α_k and θ are the parameters in k-th iteration with $\theta \in (0, 1)$, J_k is the Jacobian matrix of the magnetic mapping functions, F_k is the output of k-th magnetic mapping function. For updating each step of the parameter, a greedy strategy that pursuits the minimum error occurring in the worst direction of magnetic field is adopted. After 30 iterations, a relative better solution (Objective <1) is obtained and used as the initial solution of the WOA for further optimization. The solution of the whole process is conducted in MATLAB (MathWorks , Inc)

2) Fitting data and rotation transformation

In the proposed model , the working space $(20 \times 20 \times 20\,\text{mm}^3)$ needs to be partitioned with $21 \times 21 \times 21$ grid. To reduce the calculation time of the model, $5\times5\times5$ points from the whole data is used as the training set to solve the mapping

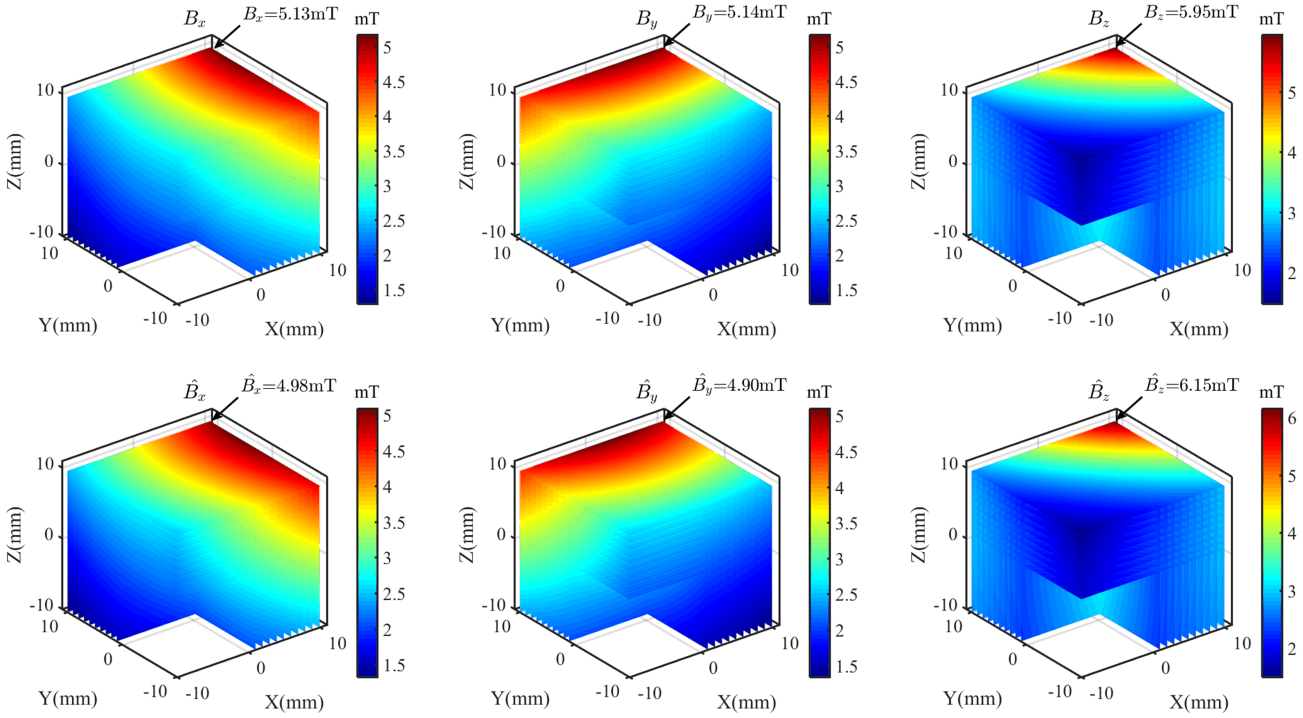

Fig. 2. *Top:* Magnetic field mapping (mT) through FEA. *Bottom:* Magnetic field mapping (mT) through the proposed model. The input current is 1A. The mapping space is $20 \times 20 \times 20\,\text{mm}^3$, and each mapping slice is separated by 1 mm.

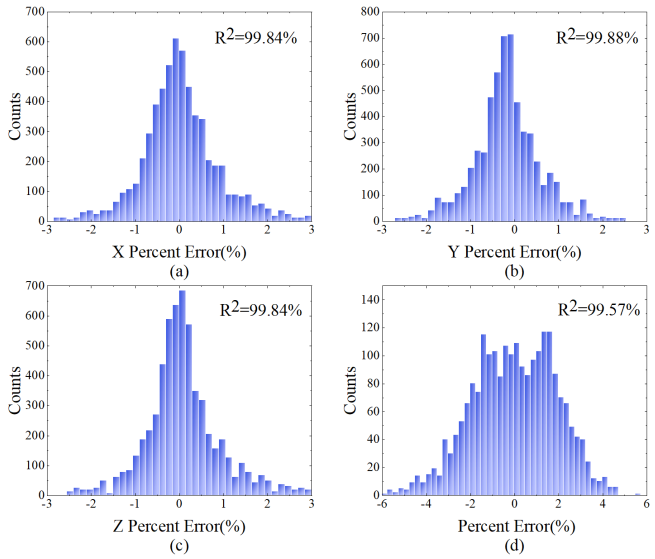

Fig. 3. (a)-(c)The distribution histogram of the relative error of the magnetic mapping vector. The worst standard deviation of the residual errors is 0.99% of the average field intensity and all R^2 values are greater than 99.81%. (d)The relative error histogram between the actual magnetic field vector of the system and the model, the maximum relative error is 7.04% with R^2 value of 99.57%.

model, the rest of the data was used to verify the accuracy of the model. While the Laplace operator has the rotation invariance, the coordinate of the working space is freely selected. Thus the model takes the rotation transformation into account, which will improve the mapping accuracy. On the other hand, when the magnetic field is measured in free space, there are anguler errors between Gaussmeter and the base. In order to fix this problem, the initial data needs to perform the rotation transformation as

$$\begin{bmatrix} B_{mx}(\mathbf{P},I) \\ B_{my}(\mathbf{P},I) \\ B_{mz}(\mathbf{P},I) \end{bmatrix} = \begin{bmatrix} r_{11} & r_{12} & r_{13} \\ r_{21} & r_{22} & r_{23} \\ r_{31} & r_{32} & r_{33} \end{bmatrix}^T \begin{bmatrix} {B^0}_{mx}(\mathbf{P},I) \\ {B^0}_{my}(\mathbf{P},I) \\ {B^0}_{mz}(\mathbf{P},I) \end{bmatrix} \quad (14)$$

and

$$\begin{bmatrix} r_{11} & r_{12} & r_{13} \\ r_{21} & r_{22} & r_{23} \\ r_{31} & r_{32} & r_{33} \end{bmatrix} = X(\alpha)Y(\beta)Z(\gamma)$$

where B^0 indicates the original data extracted from the FEA or measured data and XYZ means the rotation matrix with respect to Euler angle α, β, γ.

3)Number K selection

Although the mapping model has been built, the number K needs still to be determined. In order to minimize the objective function, a comparison test based on LMA through 30 iterations evaluation has been carried out. A total of 750 sample points with current from -3A to 3A in FEA (COMSOL, Inc., Burlington, U.S.A) is set as the input data of the model. A larger K will cause over-fitting and increase the computation time. As a result, $K = 8$ is chosen as the parameter of the model with Root-mean-square error (Rmse) of 0.109 mT.

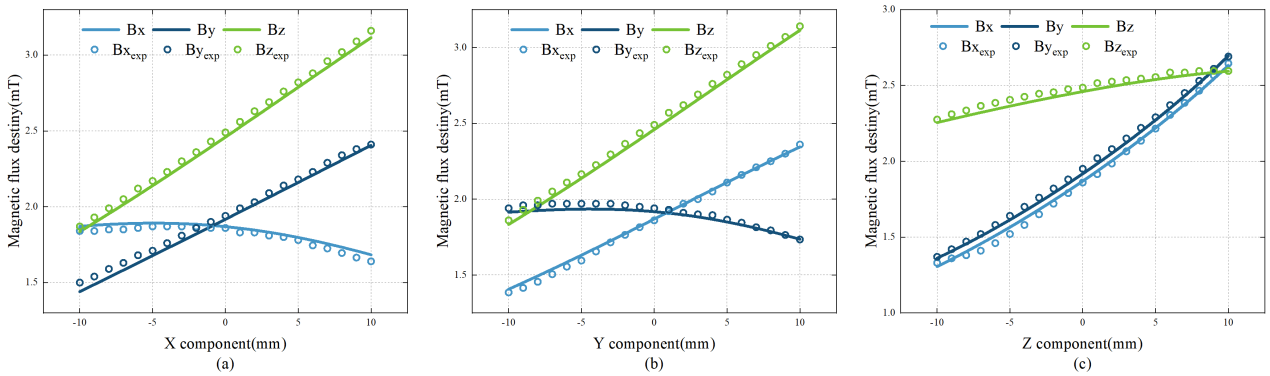

Fig. 4. (a)-(c) Comparison of the magnetic field from the experiment and the proposed model in the x-,y-,z- direction at different point. (a) x=[-10, 10], y=0, z=0. (b)x=0, y=[-10, 10] z=0. (c) x=0, y=0, z=[-10, 10].

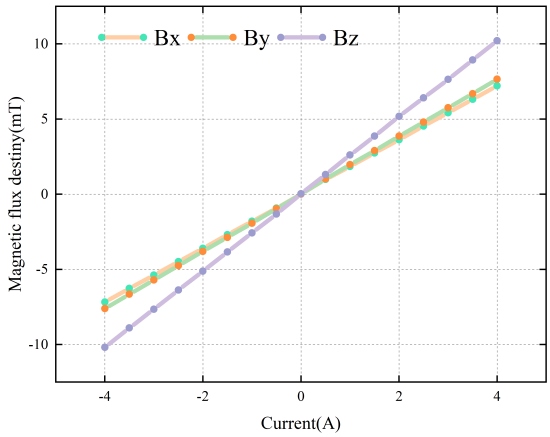

Fig. 5. Magnetic field vector generated by single coil at the point $[0, 0, 0]^T$, as the input current changes in [-4,4] A.

IV. Numerical And Experimental Result

A. Numerical result

The eight-coil magnetic manipulation system (with iron core) model is built in the FEA software. The analysis from the proposed model is conducted to obtain the numerical results. With $K = 8$, there are 84 constants (with three Euler angles) in the mapping model needs to be solved. The input current ranging from [-3, +3] A is used to calibrate the linearity of the system. A validation for a total of 6000 data points is collected as shown in Fig. 2 and Fig. 3(a)-(c).

For the calibrated magnetic manipulation system, the standard deviation of the residual errors in the x-,y-,z- directions are 0.99%, 0.79%, 0.93% of the average field amplitude, respectively. And the coefficient of determination R^2 is all greater than 99.81%. The maximum relative error is 4.02% and the relative error of 99.1% of the samples is less than 3%. The Euler angles of the three axes are all less than 0.0024°.

B. Experimental result

In the experiment, a set of devices for measuring the magnetic field was built, and it contains a three-axis high-precision Gaussmeter (G93, Coliy Technology GmbH) with the accuracy value of 1%. The resolution of the moving platform (LV-112W, Chuo Precision Industrial) can reach 0.02 mm. The power supply used in the experiment (MS3010D MAIASHENG) can output 0-5A current. Similarly, the current input in the experiment ranges in [-3,+3] A. While the measured data is limited to a 5x5x5 grid. Same as the numerical simulation test, the experiment still considers the existence of Euler angle transformation. Different from the numerical simulation, the DC offset in the x-, y-, z-directions affects the accuracy of the model, so there are 3 new solution parameters. In the measurement, a total of 750 data points were obtained for calibration. Comparison of actual measurement and model results is shown in Fig. 4. The calibration result shows that the smallest R^2 value in the three directions is 99.57% in Fig. 3(d), and the maximum relative error is 7.04%. The rotation Euler angles of x-, y-, z- directions are less than 0.05 °.

C. Linearity of the system

When building the magnetic field mapping model, it is assumed that the magnetic field generated by each electromagnet is linearly related to the current. To verify the hypothesis, an experiment on the relationship between the current input and the magnetic field was performed. In this experiment, the current of the coil changes from -4 A to +4 A with an increment of 0.5 A, and the measured value is the magnetic field vector in the Cartesian coordinate system. The result of the measurement is shown in Fig. 5. The obtained data is used for linear regression, and the coefficient of determination is close to 1, indicating that the linearity of the system is excellent.

V. Manipulation of a Permanent Magnet

When a permanent magnet or a magnetic dipole with magnetic moment $\mathbf{m}$ ($\mathrm{A{\cdot}m^2}$) placed in the magnetic manipulation system, three-dimensional magnetic force and torque will be applied to the motion and orientation of microobject [24].

$$\mathrm{F}_m = \nabla(\mathbf{m} \cdot \mathbf{B}(\mathbf{P}, I)) \tag{15}$$

$$\mathrm{T}_m = \mathbf{m} \times \mathbf{B}(\mathbf{P}, I) \tag{16}$$

where $\mathrm{F}_m, \mathrm{T}_m$ is the magnetic force and torque, $\mathbf{P}$ is the position of the magnetic object and I is the input current

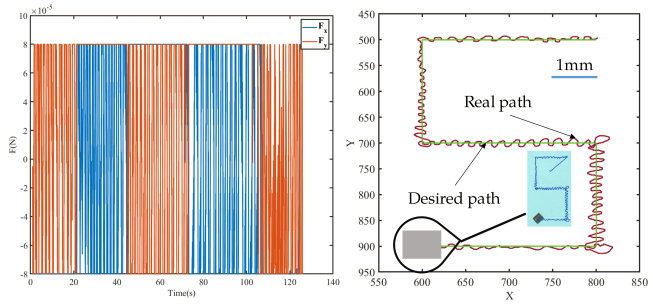

Fig. 6. *Left:* The magnetic force on the xoy plane changes with time. *Right:* Comparison of the desired path of the and the real path in the experiment.

of system. Since the mapping between magnetic field and current is clear, and the instantaneous magnetic moment $||\mathbf{m}||$ is considered constant, the system can generate a desired magnetic field by adjusting the current to actuate the magnetic object. When the object is moving in fluid, hydrodynamic drag will be generated by the fluid. The value of drag force is related to drag coefficient and speed of motion [25]:

$$\mathrm{F}_d = \frac{1}{2} C_d \rho A v^2 \tag{17}$$

where v is the flow velocity of the magnetic object, A is cross-sectional area of the object, ρ is the density of the fluid. C_d is the drag coefficient with respect to the Reynolds number. If the buoyancy and gravity are not considered in the two-dimensional plane, the dynamic equation can be expressed as follows

$$m\frac{d^2\mathbf{P}}{dt^2} = \mathbf{F}_{\mathrm{m}} + \mathbf{F}_{\mathrm{d}} + \mathbf{F}_{\mathrm{f}} + \delta \tag{18}$$

δ is random disturbance in two-dimension space, which is caused by the vibration of the system. $\mathbf{F}_{\mathrm{f}}$ is solid friction between magnetic object and petri dish. At the same time, although the current input of the system has PI feedback, the random change of the current will also affect the stability of the magnetic field when the output current is large.

The manipulation system used in the experiment is shown in Figure 1. The length of the NdFeB cylindrical permanent magnet (N38) is 1 mm and the diameter is also 1mm. The entire experiment is carried out in a petri dish filled with silicone oil, and the kinematic viscosity of the silicone oil is 1 pa·s. In this experiment, the permanent magnet is controlled by PID. After several practical tests, the parameters selected are $\mathbf{Kp}$=6 $\mathbf{Ki}$=0.6 $\mathbf{Kd}$=1. The desired path is chosen as the letter $\mathbf{S}$. In order to cope with the electronic restrictions of the system, the upper and lower limits of the magnetic force are set at 80 μN. The magnetic force changes and motion path during the experiment are shown in Fig. 6. The average speed of the whole motion process is 0.16 mm/s, and the maximum error of deviation from the desired path is 0.36 mm.

VI. Conclusion

Based on the magnetic field mapping, a flexible calibration model for the magnetic manipulation system is proposed, and the calibration results are applied to the control of the magnetic object. The influence of the proximity of the magnetic source and the hard iron effect on the magnetic field generated by a single electromagnet is taken into consideration in the system, and the mapping relationship between the magnetic field of the input current is calibrated for linearity. The model is verified on the magnetic manipulation system, and both the simulation test by the FEA and the actual measurement data have high R^2 value that are greater than 99.5%. Theoretically, our model can be used for magnetic field mapping of magnetic sources with asymmetric structures, improving the adaptability of the magnetic mapping algorithm for the development of a more advanced magnetic manipulation system.

References

[1] C. Hu, S. Pané, and B. J. Nelson, "Soft micro-and nanorobotics," *Annual Review of Control, Robotics, and Autonomous Systems*, vol. 1, pp. 53–75, 2018.

[2] M. Sitti, H. Ceylan, W. Hu, J. Giltinan, M. Turan, S. Yim, and E. Diller, "Biomedical applications of untethered mobile milli/microrobots," *Proceedings of the IEEE*, vol. 103, no. 2, pp. 205–224, 2015.

[3] X.-Z. Chen, M. Hoop, F. Mushtaq, E. Siringil, C. Hu, B. J. Nelson, and S. Pané, "Recent developments in magnetically driven micro-and nanorobots," *Applied Materials Today*, vol. 9, pp. 37–48, 2017.

[4] M. P. Kummer, J. J. Abbott, B. E. Kratochvil, R. Borer, A. Sengul, and B. J. Nelson, "Octomag: An electromagnetic system for 5-dof wireless micromanipulation," *IEEE Transactions on Robotics*, vol. 26, no. 6, pp. 1006–1017, 2010.

[5] A. W. Mahoney and J. J. Abbott, "Five-degree-of-freedom manipulation of an untethered magnetic device in fluid using a single permanent magnet with application in stomach capsule endoscopy," *The International Journal of Robotics Research*, vol. 35, no. 1-3, pp. 129–147, 2016.

[6] Z. Yang and L. Zhang, "Magnetic actuation systems for miniature robots: A review," *Advanced Intelligent Systems*, vol. 2, no. 9, p. 2000082, 2020.

[7] X. Wang, C. Hu, L. Schurz, C. De Marco, X. Chen, S. Pané, and B. J. Nelson, "Surface-chemistry-mediated control of individual magnetic helical microswimmers in a swarm," *ACS nano*, vol. 12, no. 6, pp. 6210–6217, 2018.

[8] Y.-L. Liu, D. Chen, P. Shang, and D.-C. Yin, "A review of magnet systems for targeted drug delivery," *Journal of Controlled Release*, vol. 302, pp. 90–104, 2019.

[9] D. Folio and A. Ferreira, "Two-dimensional robust magnetic resonance navigation of a ferromagnetic microrobot using pareto optimality," *IEEE Transactions on Robotics*, vol. 33, no. 3, pp. 583–593, 2017.

[10] D. Li, F. Niu, J. Li, X. Li, and D. Sun, "Gradient-enhanced electromagnetic actuation system with a new core shape design for microrobot manipulation," *IEEE Transactions on Industrial Electronics*, vol. 67, no. 6, pp. 4700–4710, 2019.

[11] F. Ongaro, S. Pane, S. Scheggi, and S. Misra, "Design of an electromagnetic setup for independent three-dimensional control of pairs of identical and nonidentical microrobots," *IEEE Transactions on Robotics*, vol. 35, no. 1, pp. 174–183, 2019.

[12] M. P. Armacost, J. Adair, T. Munger, R. R. Viswanathan, F. M. Creighton, D. T. Curd, and R. Sehra, "Accurate and reproducible target navigation with the stereotaxis niobe® magnetic navigation system," *Journal of Cardiovascular Electrophysiology*, vol. 18, pp. S26–S31, 2007.

[13] H. Takeda, T. Kubo, K. Kusaka, H. Suzuki, N. Inabe, and J. A. Nolen, "Extraction of 3d field maps of magnetic multipoles from 2d surface measurements with applications to the optics calculations of the large-acceptance superconducting fragment separator bigrips," *Nuclear Instruments & Methods in Physics Research*, vol. 317, no. pt.B, pp. 798–809, 2013.

[14] L. Huang and S. Lee, "Study on magnetic field mapping method in the center volume of the air-core solenoid," *IEEE Transactions on Applied Superconductivity*, vol. 26, no. 4, pp. 1–4, 2016.

[15] S. Schuerle, S. Erni, M. Flink, B. E. Kratochvil, and B. J. Nelson, "Three-dimensional magnetic manipulation of micro-and nanostructures for applications in life sciences," *IEEE Transactions on Magnetics*, vol. 49, no. 1, pp. 321–330, 2012.
[16] A. J. Petruska, J. Edelmann, and B. J. Nelson, "Model-based calibration for magnetic manipulation," *IEEE Transactions on Magnetics*, vol. 53, no. 7, pp. 1–6, 2017.
[17] G. Baek, J. Kim, T. K. Ko, and S. Lee, "Artificial neural network interpolation for magnetic field mapping in an air-core hts quadruple magnet," *Cryogenics*, vol. 107, p. 103043, 2020.
[18] S. Yuan, Y. Wan, and S. Song, "Rectmag3d: A magnetic actuation system for steering milli/microrobots based on rectangular electromagnetic coils," *Applied Sciences*, vol. 10, no. 8, p. 2677, 2020.
[19] E. P. Furlani, *Permanent Magnet and Electromechanical Devices: Materials, Analysis, and Applications*. Academic press, 2001.
[20] S. Mirjalili and A. Lewis, "The whale optimization algorithm," *Advances in Engineering Software*, vol. 95, pp. 51–67, 2016.
[21] D. W. Marquardt, "An algorithm for least-squares estimation of nonlinear parameters," *Journal of the Society for Industrial and Applied Mathematics*, vol. 11, no. 2, pp. 431–441, 1963.
[22] J. Y. Fan, "A modified levenberg-marquardt algorithm for singular system of nonlinear equations," *Journal of Computational Mathematics*, vol. 21, no. 5, pp. p.625–636, 2003.
[23] L. Yang and Y. P. Chen, "A new globally convergent levenberg - marquardt algorithm for solving nonlinear systems of equations," *Mathematica Numerica Sinica*, vol. 30, no. 04, pp. 388–396, 2008.
[24] A. Ghanbari, P. H. Chang, B. J. Nelson, and H. Choi, "Magnetic actuation of a cylindrical microrobot using time-delay-estimation closed-loop control: modeling and experiments," *Smart Materials & Structures*, vol. 23, no. 3, p. 035013, 2014.
[25] J. B. Mathieu, G. Beaudoin, and S. Martel, "Method of propulsion of a ferromagnetic core in the cardiovascular system through magnetic gradients generated by an mri system." *IEEE Transactions on Biomedical Engineering*, vol. 53, no. 2, pp. 292–9, 2006.